Available online at www.sciencedirect.com

ScienceDirect

Proceedings of the Combustion Institute 37 (2019) 2259–2266

Proceedings of the Combustion Institute

www.elsevier.com/locate/proci

Data assimilation using high-speed measurements and LES to examine local extinction events in turbulent flames

Jeffrey W. Labahn [a], Hao Wu [a], Bruno Coriton [b], Jonathan H. Frank [b], Matthias Ihme [a,*]

[a] *Department of Mechanical Engineering, Stanford University, Stanford, CA 94305, United States*
[b] *Combustion Research Facility, Sandia National Laboratories, Livermore, CA 94550, United States*

Received 1 December 2017; accepted 3 June 2018
Available online 24 June 2018

Abstract

Data assimilation techniques are investigated to determine how high-speed experimental measurements can be infused into a combustion simulation with the goal of capturing transient combustion events and isolating model deficiencies. To this end, an ensemble Kalman filter (EnKF) is employed to assimilate simultaneous measurements from tomographic PIV and OH-PLIF into a combustion LES of a turbulent DME jet flame, taking into consideration experimental uncertainties and modeling errors. It is shown that by assimilating experimental data, EnKF improves the prediction of the extinction and reignition dynamics observed in this flame. Subsequently, the capability of the assimilation method in evaluating the model performance is examined by considering an assimilation sequence. It is shown that the combustion model investigated (namely a flamelet/progress variable model) exhibits a tendency to relax towards a more reactive state, indicating a deficiency in quantitatively predicting the extent of extinction and reignition with this particular model.

Keywords: Data assimilation; Ensemble Kalman filter; Turbulent combustion; Extinction and reignition; Large-eddy simulation

1. Introduction

With the development of high-fidelity modeling capabilities and the increasing availability of computational resources, large-eddy simulation (LES) techniques have been demonstrated to provide improved statistical descriptions of scalar mixing, heat release, and pollutant formation in simulations of turbulent reacting flows. However, the ability of current combustion simulations to accurately describe transient combustion processes is limited for several reasons. First, these flows are inherently chaotic, so that solution trajectories diverge in time due to the exponential growth of

* Corresponding author.
E-mail address: mihme@stanford.edu (M. Ihme).

https://doi.org/10.1016/j.proci.2018.06.043
1540-7489

small perturbations [1,2]. Apart from numerical errors that are introduced through the discretization, these perturbations also arise from uncertainties in boundary conditions or incomplete specifications of the initial state. Second, physical models for the representation of turbulence/chemistry interaction, turbulent scalar fluxes, and subgrid contributions rely on model approximations, which limit their applicability to specific combustion regimes. Finally, incomplete understanding at a fundamental level introduces model deficiencies in accurately capturing particular combustion-physical mechanisms and precursor events.

Recent advances in the development of multi-dimensional high-speed measurement diagnostics have contributed to the improved understanding of combustion processes [3]. These measurements provide quantitative information about instantaneous velocity fields, temperature, and species at acquisition rates and spatial resolutions required to resolve relevant turbulent scales. This enables the examination of dynamically unsteady combustion processes, including flame-structure analysis of highly turbulent premixed flames [4], the characterization of extinction and reignition processes in non-premixed flames [5–8], and lean blowout dynamics in gas-turbine combustors [9], among others. Although these measurements have been used in evaluating combustion models, this has been largely limited to comparisons of statistical results. As such, the modeling community has not taken full advantage of the plethora of high repetition-rate measurements for analyzing the model performance or improving the model accuracy.

Data assimilation (DA) provides opportunities to integrate measurements into numerical simulations [10], and has been used extensively to produce initial conditions for weather prediction models and to provide representations of the spatio-temporally evolving atmospheric state [11]. These assimilation techniques are used to obtain an estimate of the state of a complex, spatio-temporally evolving system based on observations and a model of the dynamics of the system [12]. Data assimilation can spread information from observations in space and time to unobserved state quantities, filter the effect of random observation noise from state estimates, provide estimates of observation and model errors, and determine unknown or uncertain model parameters. Different DA-techniques have been developed [13,14] that can be categorized into variational techniques such as nudging, adjoint methods, and 3D/4D-Var, and statistical techniques such as optimal interpolation and the class of Kalman-filtering methods. While variational techniques rely on optimal control theory to minimize a deterministic cost function, statistical techniques incorporate stochastic information in the form of probability distributions of model uncertainties and observation errors. Because of the advantage of incorporating quantities not contained in the solution vector, the applicability to large-scale problems, and the robust evaluation of the error covariance, the ensemble Kalman filter is selected for data assimilation in the present work.

While data assimilation is a mature technique in the atmospheric sciences, this method has found only limited application to engineering research areas [15–18]. Evaluating the feasibility of using this technique for combustion applications is the objective of this research. Specifically, we investigate how data assimilation can be used to integrate measurements with simulations. To this end, high-speed high-resolution experimental data obtained for a turbulent partially-premixed flame [7,19] is assimilated to evaluate the performance of an LES combustion model in improving the short-term prediction of extinction and reignition events. For this, we consider a flamelet-based combustion model in which all thermochemical quantities are parameterized in terms of mixture fraction and a reaction progress variable. The experimental data set provides high spatially and temporally resolved simultaneous measurements from tomographic PIV (TPIV) and planar OH-LIF in the shear layer of the jet. Our first objective is to determine how experimental measurements of quantities not contained in the state vector (such as OH, heat-release, or chemiluminescence data) can be infused into the numerical model. With this, the second objective is to examine the impact of assimilated measurements on improving short-term predictions of the OH-LIF signal and the velocity field under consideration of experimental uncertainties and spatial data-locality. By considering a flamelet/progress variable (FPV) combustion model, the third objective is to employ DA to identify limitations of this model in predicting local extinction and reignition events.

The remainder of this paper has the following structure. The mathematical models and the data assimilation technique are discussed in Section 2. The experimental configuration and computational setup are presented in Section 3. Simulation results are examined in Section 4, and the paper finishes by drawing conclusions about the utility of using data assimilation for combustion simulations.

2. Mathematical models

2.1. Governing equations and mathematical model

The present work is concerned with LES of a turbulent reacting flow, and the FPV-model [20,21] is used to evaluate the thermochemical state. The LES utilizes a fully compressible formulation, solving the Favre-filtered conservation equations for mass, momentum, and energy.

The subgrid-scale turbulence/chemistry interaction is accounted for using a presumed PDF-model [20,21], so that all thermochemical quantities are parameterized in terms of $\widetilde{Z}$, $\widetilde{Z''^2}$, and $\widetilde{C}$, requiring the solution of corresponding transport equations. With this, the system of governing equations can be written in operator form as

$$\overline{\rho}\widetilde{D}_t\boldsymbol{\phi} = \mathcal{M}(\boldsymbol{\phi}), \tag{1}$$

where $\widetilde{D}_t$ denotes the substantial derivative, $\mathcal{M}$ represents the right-hand-side of the governing equations and $\boldsymbol{\phi} = (\overline{\rho}, \widetilde{\boldsymbol{u}}, \widetilde{e}, \widetilde{Z}, \widetilde{Z''^2}, \widetilde{C})^{\mathsf{T}}$ is the LES state vector, with ρ being the density, $\boldsymbol{u}$ the velocity vector, and e the specific total energy. Further details on the model and the numerical implementation can be found in [22]. In the current work, an un-normalized progress variable is utilized and defined as $C = Y_{CO_2} + Y_{CO} + Y_{H_2} + Y_{H_2O}$ [23]. To assimilate OH measurements into the simulation, we compute a quantitative OH-LIF signal, S_{OH}, following the approach in [24]. This signal is normalized by the mean peak value at $x/D = 20$. The OH-LIF signal is then pretabulated and evaluated from the chemistry table as $\mathcal{F}_{OH}(\widetilde{Z}, \widetilde{Z''^2}, \widetilde{C})$.

To further assess the FPV-model, we also consider an equilibrium flamelet model (EFM), which only contains a single equilibrium flamelet so that the thermochemical state is fully specified by $\widetilde{Z}$ and $\widetilde{Z''^2}$.

2.2. Data assimilation and ensemble Kalman filter

In this work, DA is employed to integrate measurements into simulations. Fundamentally, given a set of measurements of the system over a time interval, DA determines the state-space trajectory that best fits the observations in a maximum likelihood sense.

In this work, we consider the ensemble Kalman filter (EnKF), which estimates the state vector of the kth ensemble member, $\boldsymbol{\phi}_k^a(t)$, by updating its prior estimate $\boldsymbol{\phi}_k^p(t)$ with information from a perturbed observation vector $\boldsymbol{\psi}_k(t)$ through the following analysis step [10]

$$\boldsymbol{\phi}_k^a(t) = \boldsymbol{\phi}_k^p(t) + \mathbf{K}\left[\boldsymbol{\psi}_k(t) - \mathcal{H}\left(\boldsymbol{\phi}_k^p(t)\right)\right], \tag{2}$$

where the term in square brackets is the innovation, $\mathcal{H}(\boldsymbol{\phi}_k^p)$ is the observation operator, which maps the prior state vector into the vector of observables, and the observation vector combines the measurements and observation errors that are sampled from a normal distribution with expectation $\mathbf{0}$ and covariance matrix $\mathbf{R}(t)$. Equation (2) is solved for an ensemble with $k = 1, \ldots, N$, where N is the number of ensemble members. In the present work, we consider simultaneous, high-resolution measurements of the 3D velocity field and OH-PLIF signals, so that the observation vector is defined as $\boldsymbol{\psi} = (\boldsymbol{u}^{Exp}, S_{OH}^{Exp})^{\mathsf{T}}$. Following the assimilation step, the state vector is advanced in time via Eq. (1) with initial conditions $\boldsymbol{\phi}_k^a(t)$. The Kalman gain matrix, $\mathbf{K}$, is given by

$$\mathbf{K} = \mathbf{P}\mathbf{H}^{\mathsf{T}}\left(\mathbf{H}\mathbf{P}\mathbf{H}^{\mathsf{T}} + \mathbf{R}\right)^{-1}, \tag{3}$$

where $\mathbf{P}$ is the background error covariance matrix, $\mathbf{R}$ is the observation covariance error, and $\mathbf{H}$ is the Jacobian of the observation operator with respect to the state vector, $\mathbf{H} = \partial_{\boldsymbol{\phi}}\mathcal{H}(\boldsymbol{\phi})$, defined as

$$\mathbf{H} = \begin{bmatrix} 0 & 1 & 0 & 0 & 0 & 0 & 0 & 0 \\ 0 & 0 & 1 & 0 & 0 & 0 & 0 & 0 \\ 0 & 0 & 0 & 1 & 0 & 0 & 0 & 0 \\ 0 & 0 & 0 & 0 & 0 & \partial_{\widetilde{Z}}\mathcal{F}_{OH} & 0 & \partial_{\widetilde{C}}\mathcal{F}_{OH} \end{bmatrix}. \tag{4}$$

In the current EnKF approach, the density and $\widetilde{Z''^2}$ are not updated through Eq. (2), which is done to prevent the possibility of negative densities and artificially high variances; instead these quantities are advanced by their respective governing equations. The specific total energy is updated via Eq. (2) through the $\mathbf{P}$ matrix, determined as $\mathbf{P} = (N-1)^{-1}\sum_{k=1}^{N}(\boldsymbol{\phi}_k - \langle\boldsymbol{\phi}\rangle)(\boldsymbol{\phi}_k - \langle\boldsymbol{\phi}\rangle)^{\mathsf{T}}$, where $\langle\boldsymbol{\phi}\rangle$ is the mean of all ensembles.

The observation error $\mathbf{R}$ is assumed to be known and consists of different sources of errors. In the present work, errors associated with measurement noise, thermophoretic diffusion and volume reconstruction errors, have been determined from experiments at approximately 5% [7]. Additional errors due to beam steering are estimated to be below 5% [8]. Finally, uncertainties due to the inherent spatial and temporal averaging of PIV and the apparent transport of ghost particles are taken as 5%. Based on these estimates, the overall uncertainty for the velocity components is estimated at 9%. The uncertainty in the OH measurements is estimated at 10%.

3. Experiments and computational setup

3.1. Experimental configuration and data acquisition

The experimental configuration considered in this work is the piloted jet burner operated with a dimethyl ether (DME)/air mixture (Flame D) [19] issuing from a nozzle with diameter $D = 7.45$ mm at a mean exit velocity of $U_J = 45.9$ m/s, resulting in a jet exit Reynolds number of approximately 29,300. The flame was stabilized by an 18.2 mm diameter annular pilot flame, and the entire burner was surrounded by an air coflow with an exit velocity of 0.9 m/s.

Detailed descriptions of the OH-PLIF and TPIV systems including velocity uncertainty estimates are available in Refs. [7,8], and a brief overview is given here. The OH-PLIF system used a 10-kHz repetition rate Nd:YAG-pumped dye laser. The OH-PLIF signal was recorded using

an intensified high-speed CMOS camera with a projected pixel size of $37 \times 37\,\mu m^2$. The TPIV system consisted of a diode-pumped dual-head Nd:YAG laser and a set of four high-speed CMOS cameras. Measurements were performed at a repetition rate of 10 kHz. The center of the imaged region was located 20 diameters downstream of the nozzle exit, and the dimension of the probe volume is $11.4 \times 16.9 \times 3.3$ mm^3 (axial, radial, depth) and contains $128 \times 189 \times 38$ vectors with 90 μm spacing.

3.2. Computational setup

The computational domain of size $77D \times 13D \times 2\pi$ is discretized using an unstructured hexahedral mesh with approximately four million cells. The mesh is refined near the nozzle, in the shear layer and in the measurement region, which is centered at $(x/D, r/D, \theta) = (20, 1.5, 0)$ with corresponding dimensions of the 3D measurement volume.

The assimilation step, Eq. (3), is inexpensive compared to computing the LES, so that the overall cost scales approximately linearly with the number of ensembles. In the current work, the background error covariance matrix, **P**, is calculated from twelve ensemble members (that is $N = 12$), and each ensemble was initialized from solutions of a separate simulation at sufficiently decorrelated time instances. By considering an LES ensemble, a representative statistical estimate of the LES dynamics is obtained. The ensemble size is limited by computational resources, and similar numbers have been used in previous EnFK simulations [25]. Each ensemble member is advanced independently for a duration of 0.1 ms, after which time the experimental data is assimilated using the EnKF algorithm described in Section. 2.2. During the data assimilation step, EnKF-localization is applied to improve stability of the algorithm and to eliminate spurious correlations due to sampling errors [25]. It should be noted that as the DA-results are constructed, taking into account experiments and an LES-ensemble, the result is no longer a statistically independent sample.

4. Results

4.1. Flow field analysis

Before evaluating the impact of the EnKF algorithm on the time-resolved evolution of the velocity field and OH-LIF signal, it is important to ensure that the LES-model captures statistical flow-field quantities. For this, statistical results for temperature, mixture fraction, axial velocity and OH-signal are collected from LES calculations. Comparisons of radial profiles for mean and root-mean-square (rms) of temperature, mixture fraction, axial velocity, and OH-LIF signal at $x/D = 20$ from simulations and experiments are presented in Fig. 1. These results show that the predictions from the LES utilizing the FPV combustion model are in good agreement with measurements, and in good correspondence with previous simulations [24,27]. The present simulation produces a narrower OH-LIF signal compared to the experimental measurements but correctly predicts the peak location. Given that the LES is able to reproduce the statistical flame behavior at $x/D = 20$ motivates the question of whether the FPV model is able to capture the localized extinction and reignition observed in this flame with the help of DA.

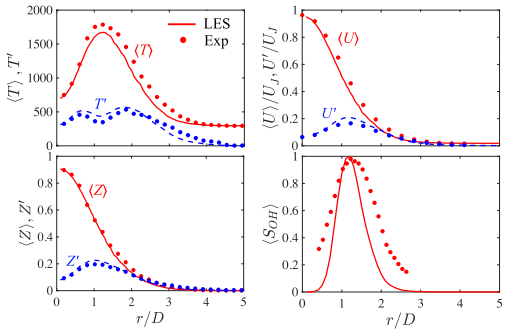

Fig. 1. Comparisons of radial profiles of mean and root-mean-square (rms) quantities of temperature, mixture fraction, axial velocity and OH-LIF signal at $x/D = 20$ from LES and measurements [19,26].

4.2. Data assimilation

Following the comparisons of statistical results, we proceed by investigating the ability of the current simulation to predict extinction and reignition. In addition, the impact of data assimilation, through EnKF, is scrutinized to determine if improvements in the transient prediction of axial velocity and OH signal can be achieved. This information can potentially be employed in isolating deficiencies in the current modeling approach and in understanding underlying phenomena responsible for extinction and reignition. For this, we employ the EnKF-technique to locally assimilate time-resolved measurements of the 3D velocity field (from TPIV) and OH-LIF signal (from OH-PLIF) into the LES.

4.2.1. Time-resolved velocity measurements

Accurately reproducing the instantaneous velocity field is crucial to capture strain rate variations, which are a main mechanism for local extinction [8]. Time-resolved axial velocity predictions at a fixed point in the measurement window obtained with and without DA are compared to the experimental data to determine if the DA-method captures this instantaneous behavior. These results

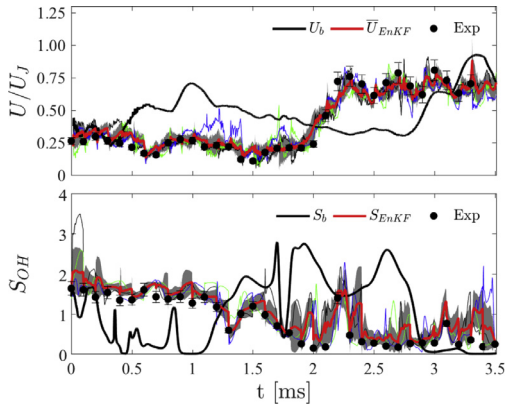

Fig. 2. Temporal evolution of axial velocity (top) and OH-LIF signal (bottom) for the baseline simulation (thick black line) and the mean obtained from the ensemble members (thick red line) compared to the experimental measurements at $(x/D, r/D, \theta) = (20, 0.961, 0.05)$. The shaded region in gray represents the rms of the ensemble members, and three representative ensemble trajectories are show by thin lines. (For interpretation of the references to color in this figure legend, the reader is referred to the web version of this article.)

are presented in Fig. 2 (top), showing axial velocity from the baseline simulations (without DA), which represents a single (stochastic) LES representation of the transient jet behavior, and velocity obtained from EnKF. It can be seen that the trajectories without DA diverge from the experimental data within less than 0.5 ms (the characteristic convective time is $\tau = D/U_J = 0.16$ ms), and the baseline simulation predicts a period of higher axial velocity followed by a period of lower velocity when compared to the measurements. It should be noted, that the baseline LES is not expected to be able to reproduce the exact transient behavior observed in Fig. 2 as LES represents a single ensemble of a stochastic process – instead it provides a reference to assess the impact that DA has on the predictions. In comparison, the twelve members of the EnKF provide a significantly better agreement with the measurements. The impact of the assimilation step is evident as there is an appreciable change in the ensemble-averaged velocity after EnKF is applied, with the ensemble-mean moving significantly closer to the experimental data. To illustrate the evolution of individual ensemble members, we show the rms of the ensemble by the gray band and trajectories of three representative members, indicating the range of velocities observed among these separate simulations. The rms is an indication of uncertainties in the numerical predictions. Note that deviations from the measurements are a direct consequence of experimental uncertainties that are considered in the Kalman gain matrix.

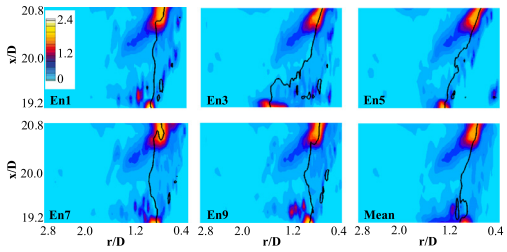

Fig. 3. OH-LIF signal for five representative instantaneous ensemble members and ensemble mean at $t = 2.0$ ms. Solid black line corresponds to the stoichiometric mixture fraction (color online).

4.2.2. Time-resolved OH measurements

To examine the capability of the DA-technique in capturing local extinction or reignition, we consider the temporal evolution of the calculated OH-LIF signal.

The temporal evolution of S_{OH}, along with instantaneous OH-fields for five ensemble members together with the ensemble mean at $t = 2$ ms are presented in Fig. 2 (bottom) and Fig. 3, respectively. As expected, the OH-signal computed from the baseline simulation shows appreciable qualitative and quantitative differences with the measurements over the course of the assimilation sequence. By assimilating measurements into simulations, the LES-calculations are in better agreement with transient OH measurements. It should be noted that even after the introduction of DA, differences between the ensemble mean and the experimental data still exist due to uncertainties in the measurements and model errors. Compared to the axial velocity predictions, the rms obtained from the ensemble members for the OH-LIF signal is much higher and changes introduced through EnKF are larger. This is a result of the consideration of experimental uncertainties in the gain matrix and the coupling of OH-data to the solution state vector through the combustion model. Instantaneous OH-LIF signal fields for five ensembles and the ensemble mean, shown in Fig. 3 at $t = 2$ ms, illustrate the variability among the ensemble members after the assimilation step. Each ensemble shares the same major flow characteristics, such as the extent of local extinction and location of the peak OH-signal. However, variations between ensembles are present throughout the assimilation window with significant variation near the centerline and in the lower half of the assimilation window.

4.2.3. Extinction and reignition dynamics

Apart from understanding the impact of EnKF on the local flow-field evolution, we are interested in evaluating the ability of the combustion model in capturing the spatio-temporal dynamics of extinction and reignition events. To assess the effectiveness of the simulation in incorporating

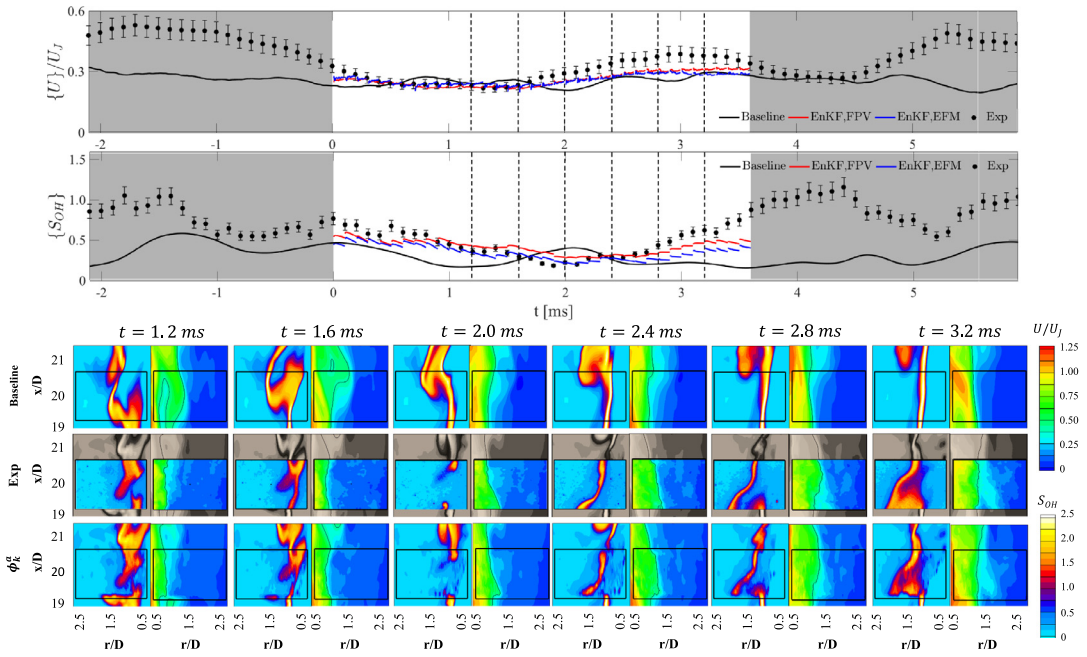

Fig. 4. Comparison of temporal evolution (top graphs) of mean axial velocity and mean OH-LIF signal within the assimilation window. Bottom: Data sequence of axial velocity (right panel) and OH-LIF signal (left panel) at six simulation times (indicated by dashed lines in the top figure). Top row: baseline simulation, middle: measurements, and bottom: results after assimilation step. Black box indicates the location of the measurement window and isocontours are $u/U_J = 0.44$ (color online).

measurements, we compute the mean axial velocity and OH-LIF signal by averaging over the measurement volume (denoted by $\{\cdot\}$) Comparisons of the temporal evolution of this mean quantity from measurements, baseline simulation, and data assimilation are illustrated in Fig. 4 (top graphs). These results show that EnKF is successfully assimilating experimental data, thereby reducing the difference between computational results and measurements.

We proceed by examining instantaneous flow-field results for OH-LIF measurements and axial velocity obtained from the baseline simulation and from one of the ensemble members. These instantaneous results are compared with measured OH-PLIF images to determine how well each simulation reproduces the local flow-field and extinction dynamics. A sequence of six experimental OH-PLIF observations, separated by $\Delta t = 0.4$ ms, is presented in Fig. 4 (bottom). Panels on the left illustrate the OH-LIF signal, and panels on the right show the instantaneous axial velocity field in the region of the measurement window. The sequence is chosen as it contains a local extinction event, which is followed by successful reignition.

At the start of the assimilation sequence, the baseline simulation produces a flame with a dramatically different flame structure as compared to the experimental data. When the experimental data is assimilated into the simulation the resulting flame structure shows better agreement with the OH-PLIF measurements. However, even after DA, differences can be observed near the flame edge in the lower right corner which we attribute to uncertainties in measurements and model deficiencies that are considered within the DA framework.

As the sequence progresses the impact of DA becomes more apparent. At all times the baseline simulation produces a flame shape which does not match the experimental observations and contains no local extinction, whereas the EnKF simulation captures the local formation of flame holes and flame recovery. A similar level of improvement is also observed for the axial velocity predictions with the introduction of DA. Compared to the baseline case, the EnKF simulations predict higher velocities past a radial distance of $r/D = 1.5$, which are in better agreement with the experimental data at each observation.

4.2.4. Model response and model evaluation

We close our discussion by examining the feedback of the measurements on the combustion model (via the independent state variables $\widetilde{Z}$ and $\widetilde{C}$) through the Kalman gain. To this end, we consider the local extinction event at $t = 2$ ms.

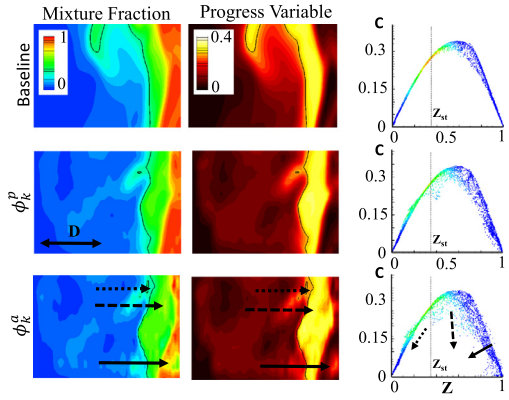

Fig. 5. Instantaneous mixture fraction (left) and progress variable (middle) fields along with scatter data (colored by OH-LIF signal, right) during the assimilation step for FPV-model. Solid line corresponds to stoichiometric isocontour; window dimensions same as in Fig. 3 (color online).

Figure 5 shows the corresponding response of the combustion model during the assimilation step. As seen from the conditional results, the baseline simulation predicts conditions that are near the equilibrium composition, without significant evidence of extinction. In contrast, during the assimilation sequence, shown in the second and third rows of Fig. 5, EnKF locally corrects the mixture fraction and progress variable to better approximate the observations (see arrows). We examine Eq. (3) to understand how information about OH-PLIF measurements are assimilated into the combustion model alone. For this, we compute the **H** matrix from the combustion model as $\mathbf{H} = \left[\partial_{\widetilde{Z}}\mathcal{F}_{\mathrm{OH}}, \partial_{\widetilde{C}}\mathcal{F}_{\mathrm{OH}}\right]$. By considering only one ensemble, this problem can be represented by a Kalman filter. With this, the update of the state-vector for the combustion model through the Kalman gain is evaluated as:

$$\begin{pmatrix} d\widetilde{Z} \\ d\widetilde{C} \end{pmatrix} = \frac{1}{\Delta}\begin{pmatrix} \partial_{\widetilde{Z}}\mathcal{F}_{\mathrm{OH}} \\ \partial_{\widetilde{C}}\mathcal{F}_{\mathrm{OH}} \end{pmatrix}\left[S_{\mathrm{OH}}^{\mathrm{Exp}} - \mathcal{F}_{\mathrm{OH}}(\widetilde{Z},\widetilde{C})\right], \qquad (5)$$

where $\Delta = \left[(\partial_{\widetilde{Z}}\mathcal{F}_{\mathrm{OH}})^2 + (\partial_{\widetilde{C}}\mathcal{F}_{\mathrm{OH}})^2 + r/p\right]$ and r/p is the ratio between observation error and background error. Equation (5) shows that the innovation directly propagates differences between measurements and simulations to the state vector, and Eq. (5) reduces to a gradient descent method. To represent extinction events, observed at $t = 2$ ms, the Kalman gain locally forces a shift to lower values of mixture fraction and progress variable to counteract the high reactivity predicted by the FPV-combustion model (see arrows in Fig. 5). Although it is known that the FPV model underpredicts extinction [28] and more advanced models can be employed, DA provides the unique opportunity for directly interrogating the instantaneous model response when exposed to data, thereby examining the model plausibility. Specifically, for this case we show that the FPV-model is mimicking local extinction by enhancing the scalar segregation and reduced reactivity. In addition, the intermittent trajectory of the mean OH-LIF signal in Fig. 4 indicates the tendency of the FPV-model to underpredict extinction, which is represented by a rapid relaxation of the FPV-model towards a more reactive state after the assimilation step.

Further assessment of the FPV-model is obtained by considering an equilibrium flamelet model (EFM), which is constructed from the equilibrium flamelet solution. A comparison of solutions between FPV and EFM is illustrated in Fig. 4 (top graphs), showing larger changes in the mean OH-signal and mean axial velocity for the EFM. This is due to EFM being unable to fully capture the extinction physics present in the current flow. The large update during the assimilation step and subsequently rapid relaxation toward its prior state can be seen for $t > 3$ ms, where the FPV-model results are much closer to the experimental data. In contrast, a smaller update is observed during the assimilation step for the FPV-model, indicating that the FPV-model provides an improved representation of the local extinction and reignition event. While this analysis illustrates the capability of employing DA for model evaluations, further work is needed to take full advantage of this method for model improvements.

5. Conclusions

In the present study, DA is utilized to assimilate data acquired from simultaneous high-speed measurements of a partially-premixed turbulent DME flame into LES. To this end, an ensemble Kalman filter, consisting of twelve ensemble members, is employed. In this LES, the combustion is represented by a flamelet/progress variable model. It is shown that the ensemble Kalman filter is able to incorporate different types of experimental measurements, commonly used in combustion diagnostics (such as TPIV, OH-PLIF), into a high-fidelity combustion simulation. The assimilation of experimental data is found to qualitatively improve the short-term prediction of the OH-LIF signal and velocity and the major characteristic observed during a local extinction sequence is recovered through the EnKF-method. However, quantitative differences in predicting the extinction intensity are observed.

The analysis of the response of the FPV-combustion model through the Kalman gain filter is investigated during an assimilation step. Through this analysis, it is shown that the innovation is propagated to the combustion state vector via the Kalman gain matrix, and is physically reflected by increased scalar mixing. The inherent assumptions of the steady-flamelet model are

causal in underpredicting the extinction strength, which is reflected by the tendency of the model to relax too fast to a more reactive state.

Acknowledgments

The authors gratefully acknowledge financial support through NASA with award NX15AV04A and the Stanford-Ford Alliance. J. H. Frank and B. Coriton gratefully acknowledge the support of the U.S. Department of Energy, Office of Science, Office of Basic Energy Sciences, Division of Chemical Sciences, Geosciences, and Biosciences. Sandia National Laboratories is a multimission laboratory managed and operated by National Technology & Engineering Solutions of Sandia, LLC, a wholly owned subsidiary of Honeywell International Inc., for the U.S. Department of Energy's National Nuclear Security Administration under contract DE-NA0003525. The views expressed in the article do not necessarily represent the views of the U.S. Department of Energy or the United States Government.

References

[1] R.C. Hilborn, Chaos and Nonlinear Dynamics: An Introduction for Scientists and Engineers, Oxford University Press, 1994.
[2] G. Nastac, J.W. Labahn, L. Magri, M. Ihme, *Phys. Rev. Fluids* 2 (2017) 094606.
[3] V. Sick, *Proc. Combust. Inst.* 34 (2013) 3509–3530.
[4] A.W. Skiba, T.M. Wabel, C.D. Carter, S.D. Hammack, J.E. Temme, J.F. Driscoll, *Combust. Flame* 189 (2018) 407–432.
[5] A.M. Steinberg, I. Boxx, C.M. Arndt, J.H. Frank, W. Meier, *Proc. Combust. Inst.* 33 (2011) 1663–1672.
[6] R.A. Patton, K.N. Gabet, N. Jiang, W.R. Lempert, J.A. Sutton, *Appl. Phys. B* 108 (2012) 377–392.
[7] B. Coriton, J.H. Frank, *Proc. Combust. Inst.* 35 (2015) 1243–1250.
[8] B. Coriton, A.M. Steinberg, J.H. Frank, *Exp. Fluids* 55 (2014) 1743.
[9] M. Stöhr, I. Boxx, C.D. Carter, W. Meier, *Proc. Combust. Inst.* 33 (2011) 2953–2960.
[10] G. Evensen, *Data Assimilation*, second ed., Springer, Berlin, 2009.
[11] E. Kalnay, *Atmospheric Modeling, Data Assimilation and Predictability*, Cambridge University Press, 2003.
[12] E. Ott, B.R. Hunt, I. Szunyogh, et al., *Tellus* 56A (2004) 415–428.
[13] P.L. Houtekamer, F. Zhang, *Mon. Weather Rev.* 144 (2016) 4489–4532.
[14] M. Asch, M. Bocquet, M. Nodet, *Data Assimilation: Methods, Algorithms, and Applications*, SIAM, 2016.
[15] A.J. Majda, J. Harlim, *Filtering Complex Turbulent Systems*, Cambridge University Press, 2012.
[16] W. Jahn, G. Rein, J.L. Torero, *Fire Safety J.* 46 (2011) 81–88.
[17] M.C. Rochoux, B. Delmotte, B. Cuenot, S. Ricci, A. Trouvé, *Proc. Combust. Inst.* 34 (2013) 2641–2647.
[18] X. Gao, Y. Wang, N. Overton, M. Zupanski, X. Tu, *J. Comput. Sci.* 21 (2017) 38–59.
[19] B. Coriton, S.K. Im, M. Gamba, J.H. Frank, *Combust. Flame* 180 (2017) 40–52.
[20] C.D. Pierce, P. Moin, *J. Fluid Mech.* 504 (2004) 73–97.
[21] M. Ihme, C.M. Cha, H. Pitsch, *Proc. Combust. Inst.* 30 (2005) 793–800.
[22] P.C. Ma, Y. Lv, M. Ihme, *J. Comput. Phys.* 340 (2017) 330–357.
[23] M. Ihme, L. Shunn, J. Zhang, *J. Comput. Phys.* 231 (2012) 7715–7721.
[24] S. Popp, F. Hunger, S. Hartl, et al., *Combust. Flame* 162 (2015) 3016–3029.
[25] C.S. Schwartz, G.S. Romine, R.A. Sobash, K.R. Fossell, M.L. Weisman, *Weather Forecast.* 30 (2015) 1645–1654.
[26] F. Fuest, G. Magnotti, R.S. Barlow, J.A. Sutton, *Proc. Combust. Inst.* 35 (2015) 1235–1242.
[27] J. You, Y. Yang, S.B. Pope, *Combust. Flame* 176 (2017) 451–461.
[28] M. Ihme, H. Pitsch, *Combust. Flame* 155 (2008) 90–107.